J. Fluid Mech. (1976), *vol.* 78, *part* 2, *pp.* 337–354
Printed in Great Britain

Thermally, mechanically or externally driven flows in a gas centrifuge with insulated horizontal end plates

BY TAKUYA MATSUDA† AND KIYOSHI HASHIMOTO

Department of Aeronautical Engineering, Kyoto University, Kyoto, Japan

(Received 22 March 1976)

The axisymmetric motion of a compressible fluid in a rapidly rotating cylinder is considered using a linear approach and boundary-layer techniques. The deviation of the fluid motion from rigid-body rotation is caused either by an applied temperature distribution on the side wall, a differential rotation of the top and bottom end plates or sources and sinks of fluid distributed on the end plates. The horizontal end plates are assumed to be thermally insulated, while the side wall is conducting. The critical parameter governing the problem is found to be $E^{-\frac{1}{2}}(\gamma-1)P_r G_0/4\gamma$, where E is the Ekman number, γ the ratio of specific heats, P_r the Prandtl number and G_0 the square of a rotational Mach number. If this parameter is larger than unity, the coupled effect of the compressibility of the fluid and the thermal condition on the end plates suppresses the flow in the cylinder. The flow in the inner inviscid core is strongly coupled with the Ekman-layer flow through the boundary conditions on the end plates, something which does not occur if the fluid is Boussinesq nor if the fluid is compressible and the end plates are conducting.

1. Introduction

The meridional flow of a compressible fluid in a rapidly rotating cylinder is the *fundamental initial state* from which investigations of uranium enrichment in a gas centrifuge proceed (Cohen 1951; Kanagawa & Oyama 1961; Olander 1972; Matsuda 1975). A counter-current flow is established by either a vertical temperature difference in a thermally driven gas centrifuge, obstacles called scoupes in a mechanically driven device or by source–sink distributions on the horizontal end plates in an externally driven device.

Thermally driven flow in a gas centrifuge was studied by Sakurai & Matsuda (1974, which will be referred to as I hereafter) and Nakayama & Usui (1974) under the assumption that all cylinder walls are thermally conducting. The case in which the side wall is thermally insulated was considered by Matsuda, Hashimoto & Takeda (1976, which will be referred to as III). Source–sink flows were

† Temporary adress: Department of Applied Mathematics and Astronomy, University College, Cardiff, Wales.

treated by Nakayama & Usui (1974), Hashimoto (1975) and Matsuda, Sakurai & Takeda (1975, which will be referred to as II).

Comparing these studies with investigations based on the Boussinesq approximation (Homsy & Hudson 1969) clarifies the following characteristics of rotating compressible fluids: (i) as the effective Ekman number is a function of the radial position r, the Ekman suction varies radially; (ii) radial motions of fluid elements produce or remove heat through the work done by the pressure, and this heat affects the dynamics of the fluid. In III, the authors found that characteristic (ii) is particularly pronounced when the cylinder walls are thermally insulated. They restricted themselves to thermally driven flow in a rotating cylinder with an insulated side wall and conducting end plates and found that the inner temperature field and the closed circulation in the $E^{\frac{1}{3}}$-layer on the side wall deviate very much from those obtained on the assumption of a conducting side wall (Sakurai & Matsuda 1974). The axial flow velocity in the inner inviscid core, however, was found to be identical to the case of a conducting side wall because in this case the axial flow velocity is not coupled with the temperature field in the inner inviscid core and is determined only by the boundary conditions on the top and bottom end plates (see III). This is peculiar to the case of conducting end plates where the temperature distribution is given. Therefore, we can expect that in a general case, insulated end plates for example, the thermal conditions on the end plates yield the coupling between the axial flow and the Ekman-layer flow through the temperature. Then the axial flow, which plays an essential role in estimating the efficiency of uranium enrichment, will be affected not only by the conditions on the end plates but also by those on the side wall.

Accordingly, in this paper we study the flow of a compressible fluid such as UF_6 gas in a very rapidly rotating cylinder with completely insulated end plates and a conducting side wall as a limiting case; the flows are driven either thermally, mechanically or externally. The critical parameter governing the solution in III was found to be $\alpha = hE^{-\frac{1}{3}}$, where E is the Ekman number defined at the periphery and $h = (\gamma-1)P_r G_0/4\gamma$ is a measure of the compressibility of the fluid (see next section). If α is larger than unity, the combined effect of the compressibility of the fluid and the insulated side wall becomes important. In a practical gas centrifuge, α was estimated to be of the order of 10. In the present problem, the critical parameter will be shown to be $\beta \equiv hE^{-\frac{1}{2}}$, which is estimated to have a value of $10^2 \sim 10^3$.

2. Formulation

Basic equations

Consider a cylinder of radius L and height $2H$ which is rotating about its vertical axis and which contains a compressible fluid such as UF_6 gas. The top and bottom end plates rotate with an angular speed $\Omega+\Delta\Omega$ and $\Omega-\Delta\Omega$, respectively, while the side wall rotates with angular speed Ω. This configuration does not exactly simulate a mechanically driven gas centrifuge; however, it is adopted for the sake of simplicity. The top and bottom end plates are thermally insulated, while a linear temperature distribution is applied on the side wall, i.e. $T = T_0+\Delta T Z/H$,

where T_0 is the mean temperature and Z varies from $-H$ to H. This temperature distribution on the side wall induces a thermally driven flow in the inner inviscid core. On the top and bottom end plates, there are circular slits through which fluid is injected or withdrawn. The axial velocity profiles are given by $W_+(r)$ and $W_-(r)$ on the top and bottom end plates, respectively, while the horizontal components of velocity are assumed zero in the rotating frame.

Assuming axisymmetry and $\Delta T/T_0 \ll 1$, we obtain the following set of linearized dimensionless equations in a manner similar to III:

$$\operatorname{div} \mathbf{q} + G_0 r u = 0, \tag{2.1}$$

$$-2v + rT + \frac{1}{G_0}\frac{\partial p}{\partial r} = \frac{E}{\epsilon_R}\left(\mathscr{L}u + \frac{1}{3}\frac{\partial}{\partial r}\operatorname{div}\mathbf{q}\right), \tag{2.2}$$

$$2u = (E/\epsilon_R)\mathscr{L}v, \tag{2.3}$$

$$\frac{1}{G_0}\frac{\partial p}{\partial z} = \frac{E}{\epsilon_R}\left(\Delta w + \frac{1}{3}\frac{\partial}{\partial z}\operatorname{div}\mathbf{q}\right), \tag{2.4}$$

$$-4hru = (E/\epsilon_R)\,\Delta T, \tag{2.5}$$

where

$$\operatorname{div}\mathbf{q} = \frac{1}{r}\frac{\partial}{\partial r}(ru) + \frac{\partial w}{\partial z}, \quad \Delta = \frac{\partial^2}{\partial r^2} + \frac{1}{r}\frac{\partial}{\partial r} + \frac{\partial^2}{\partial z^2}, \quad \mathscr{L} = \Delta - \frac{1}{r^2}, \tag{2.6}$$

$$\epsilon_R = \exp[\tfrac{1}{2}G_0(r^2-1)], \quad E = \frac{\mu}{\rho_2 \Omega L^2}, \quad G_0 = \frac{ML^2\Omega^2}{RT_0}, \quad h = \frac{(r-1)P_r G_0}{4r}. \tag{2.7}$$

In the above expressions, $\mathbf{q}(u, v, w)$, p and T are respectively the dimensionless perturbations in velocity, pressure and temperature, ρ_2 is the fluid density at the side wall, P_r the Prandtl number, M the mean molecular weight of the fluid, R the universal gas constant, γ the ratio of specific heats and μ the coefficient of viscosity. Equation (2.1) is the equation of continuity, (2.2)–(2.4) are the r, θ and z components of the equation of motion and (2.5) is the energy equation. The characteristic feature of a compressible fluid is the heat-source term contained on the left-hand side of (2.5), which is due to the work done by pressure during radial motion of the fluid. In the present work, we neglect gravity because its magnitude is about 10^{-5} times that of the typical centrifugal force in a gas centrifuge.

The appropriate boundary conditions for the present problem are

$$\partial T/\partial z = 0 \quad \text{at} \quad z = \pm A, \tag{2.8}$$

$$T = z/A \quad \text{at} \quad r = 1, \tag{2.9}$$

$$u = 0, \quad v = \pm r\omega, \quad w = w_\pm(r) \quad \text{at} \quad z = \pm A, \tag{2.10}$$

$$u = v = w = 0 \quad \text{at} \quad r = 1, \tag{2.11}$$

where $A = H/L$ and ω is the dimensionless angular speed of the end plate.

The orders of magnitude of the dimensionless parameters: $E = O(10^{-6} \sim 10^{-7})$, $G_0 = O(10)$, $h = O(10^{-1})$ and $A \sim 5$. Therefore the parameter $\beta \equiv hE^{-\frac{1}{2}}$, which plays a decisive role in the present problem, is of the order of 10^2 for a typical gas centrifuge.

Inner core

The analysis of the inner inviscid core is completely parallel to that in I, II and III. Proper scaling of (2.2) gives us the thermal geostrophic-wind relation:

$$v_i = \tfrac{1}{2}\{rT_i - f(r)\}, \tag{2.12}$$

where $f(r) = -G_0^{-1}(\partial P_i/\partial r)$ and the suffix i denotes quantities in the inner core. Note that the pressure P_i is independent of z in the inner inviscid core from (2.4). Eliminating all variables except T_i from (2.1)–(2.5), we obtain

$$(1+hr^2)\left(\frac{\partial^2}{\partial r^2}+\frac{\partial^2}{\partial z^2}\right)T_i + \frac{1+3hr^2}{r}\frac{\partial T_i}{\partial r} = hr\mathscr{L}f, \tag{2.13}$$

where

$$\mathscr{L}f = \frac{d^2f}{dr^2}+\frac{1}{r}\frac{df}{dr}-\frac{f}{r^2}.$$

The problem reduces to solving for T_i and $f(r)$ using (2.13) and the appropriate boundary conditions. The boundary conditions for T_i at $z = \pm A$ and at $r = 1$ and the explicit form of $f(r)$ are given after analysing the structures of the Ekman layers on the top and bottom end plates and the boundary layer on the side wall.

3. The analysis of the Ekman layer

In this section we study the structure of the Ekman layer to obtain the horizontal boundary conditions for T_i and the explicit form of $f(r)$. The Ekman-layer corrections to the inner flow are scaled according to

$$u = \hat{u}, \quad v = \hat{v}, \quad w = E^{\frac{1}{2}}\hat{w}, \quad T = h\hat{T}, \quad \eta = E^{-\frac{1}{2}}(A - jz), \tag{3.1}$$

where carets over letters denote the corrections in the Ekman layer, η denotes the stretched co-ordinate and j is 1 for the top plate and -1 for the bottom plate. The scaling of the temperature has been changed from that in I, II and III for the sake of convenience.

Inserting (3.1) into the basic equations (2.1)–(2.5) and retaining the lowest-order terms with respect to $E^{\frac{1}{2}}$, we obtain

$$\frac{1}{r}\frac{\partial}{\partial r}(r\hat{u}) - j\frac{\partial\hat{w}}{\partial\eta} + G_0 r\hat{u} = 0, \quad -2\hat{v} + hr\hat{T} = \frac{1}{\epsilon_R}\frac{\partial^2\hat{u}}{\partial\eta^2}, \tag{3.2), (3.3}$$

$$2\hat{u} = \frac{1}{\epsilon_R}\frac{\partial^2\hat{v}}{\partial\eta^2}, \quad -4r\hat{u} = \frac{1}{\epsilon_R}\frac{\partial^2\hat{T}}{\partial\eta^2}, \tag{3.4), (3.5}$$

where the vertical component of the equation of motion is omitted because it is not required for the present problem.

Using the order of magnitude of the quantities in the inner core and in the Ekman layer, we can rewrite the boundary conditions (2.8) and (2.10) as follows:

$$\partial T_i/\partial z - j\beta\partial\hat{T}/\partial\eta = 0, \tag{3.6}$$

$$\hat{u} = 0, \quad v_i + \hat{v} = jr\omega, \quad w_i + \hat{w} = w_{\pm}(r). \tag{3.7)–(3.9}$$

Eliminating $\hat{u}$ from (3.4) and (3.5) and noting that boundary-layer corrections must vanish as $\eta \to \infty$, we obtain

$$\hat{v} = -\hat{T}/2r. \tag{3.10}$$

Eliminating $\hat{u}$, $\hat{v}$ from (3.3)–(3.5) to obtain an equation for $\hat{T}$ yields

$$\partial^4\hat{T}/\partial\eta^4 + 4\sigma^4\hat{T} = 0, \tag{3.11}$$

where $\sigma = \{\epsilon_R^2(1+hr^2)\}^{\frac{1}{4}}$. Using (3.5), we can write the boundary condition (3.7) in terms of $\hat{T}$ as $\partial^2\hat{T}/\partial\eta^2 = 0$. Then (3.11) is easily solved to give

$$\hat{T} = C_\pm(r)\, e^{-\sigma\eta}\cos\sigma\eta \quad \text{at} \quad z = \pm A, \tag{3.12}$$

where $C_\pm(r)$ are unknown functions to be determined later by using the other boundary conditions. The solutions for the other variables are

$$\hat{u} = -(1+hr^2)^{\frac{1}{2}}(2r)^{-1}C_\pm(r)\, e^{-\sigma\eta}\sin\sigma\eta, \tag{3.13}$$

$$\hat{v} = -C_\pm(r)\,(2r)^{-1}\, e^{-\sigma\eta}\cos\sigma\eta \quad \text{at} \quad z = \pm A. \tag{3.14}$$

Substitution of (3.12) into (3.6) gives

$$\partial T_i/\partial z + j\beta\sigma(r)\,C_\pm(r) = 0 \quad \text{at} \quad z = \pm A. \tag{3.15}$$

Inserting (2.12) and (3.14) into (3.8), we obtain

$$r^2T_i - rf(r) - C_\pm(r) = 2jr^2\omega \quad \text{at} \quad z = \pm A. \tag{3.16}$$

Eliminating $C_\pm(r)$ from (3.15) and (3.16) we obtain the boundary condition for (2.13) on the top and bottom end plates:

$$r^2T_i + \frac{j}{\beta\sigma(r)}\frac{\partial T_i}{\partial z} = rf(r) + 2jr^2\omega \quad \text{at} \quad z = \pm A. \tag{3.17}$$

The axial velocity $\hat{w}$ is obtained by integrating (3.2) with respect to η:

$$\hat{w} = \frac{j(1+hr^2)^{\frac{1}{2}}}{4\sigma}C_\pm(r)\, e^{-\sigma\eta}\left[\left\{\frac{1}{rC_\pm}\frac{dC_\pm}{dr} + \frac{1}{2}G_0 + \frac{h}{2(1+hr^2)}\right\}\right.$$
$$\left.\times(\sin\sigma\eta + \cos\sigma\eta) - \frac{2}{r}\frac{d\sigma}{dr}\eta\sin\sigma\eta\right] \quad \text{at} \quad z = \pm A. \tag{3.18}$$

Substituting (3.18) into the boundary condition (3.9) and setting $\eta = 0$, we obtain the following two equations:

$$w_i + \frac{j(1+hr^2)^{\frac{1}{2}}}{8\sigma}\left\{\frac{2}{r}\frac{dC_\pm}{dr} + \left(G_0 + \frac{h}{1+hr^2}\right)C_\pm\right\} = w_\pm(r). \tag{3.19}$$

Noting the fact that, from the continuity equation (2.1), w_i is independent of z in the inviscid core, we add and subtract the two equations contained in (3.19) to obtain, respectively,

$$w_i = \tfrac{1}{2}(w_+ + w_-) - \frac{(1+hr^2)^{\frac{1}{2}}}{8\sigma}\left\{\frac{2}{r}\frac{dC_a}{dr} + \left(G_0 + \frac{h}{1+hr^2}\right)C_a\right\}, \tag{3.20}$$

$$\frac{dC_s}{dr} + \tfrac{1}{2}r\left(G_0 + \frac{h}{1+hr^2}\right)C_s = \frac{2r\sigma}{(1+hr^2)^{\frac{1}{2}}}(w_+ - w_-), \tag{3.21}$$

where $C_s(r) = \frac{1}{2}(C_+ + C_-)$ and $C_a(r) = \frac{1}{2}(C_+ - C_-)$. Equation (3.20) corresponds to the Ekman compatibility relation in an incompressible fluid. Equation (3.21) is easily solved to give

$$C_s(r) = 2\sigma(r)^{-1} \int_0^r r\epsilon_R(w_+ - w_-)\, dr, \tag{3.22}$$

where $C_\pm(0) = 0$ has been used. In order to obtain $C_a(r)$ and $f(r)$, we add and subtract the two equations in (3.16):

$$f(r) = \tfrac{1}{2}r\{T_i(r, A) + T_i(r, -A)\} - r^{-1}C_s(r), \tag{3.23}$$

$$C_a(r) = \tfrac{1}{2}r^2\{T_i(r, A) - T_i(r, -A)\} - 2r^2\omega. \tag{3.24}$$

4. The analysis of the side-wall boundary layers

The solutions in the inner inviscid core are connected with the boundary conditions on the side wall through the side-wall boundary layer. The structure of the side-wall boundary layer was studied by Stewartson (1957) and, for incompressible fluids, he found that this layer was composed of two layers with thicknesses $E^{\frac{1}{4}}$ and $E^{\frac{1}{3}}$, respectively. The extension to the case of compressible fluids is straightforward in the present parameter range.

The $E^{\frac{1}{4}}$-layer components are scaled according to

$$u = E^{\frac{1}{4}}\tilde{u}, \quad v = \tilde{v}, \quad w = E^{\frac{1}{4}}\tilde{w}, \quad T = \tilde{T}, \tag{4.1}$$

where tildes refer to the $E^{\frac{1}{4}}$-layer. Using the stretched variable ξ defined by

$$\xi = E^{-\frac{1}{4}}(r - 1), \tag{4.2}$$

we obtain the equations in the $E^{\frac{1}{4}}$-layer as

$$\partial\tilde{u}/\partial\xi + \partial\tilde{w}/\partial z = 0, \tag{4.3}$$

$$-2\tilde{v} + \tilde{T} + G_0^{-1}\,\partial\tilde{p}/\partial\xi = 0, \tag{4.4}$$

$$2\tilde{u} = \partial^2\tilde{v}/\partial\xi^2, \tag{4.5}$$

$$\partial\tilde{p}/\partial z = 0, \tag{4.6}$$

$$-4h\tilde{u} = \partial^2\tilde{T}/\partial\xi^2. \tag{4.7}$$

These equations are easily integrated and $\tilde{u}$, $\tilde{v}$, $\tilde{w}$ and $\tilde{T}$ can be expressed in terms of $\tilde{p}(\xi)$:

$$\tilde{u} = \frac{1}{4(1+h)\,G_0}\frac{d^3\tilde{p}}{d\xi^3}, \tag{4.8}$$

$$\tilde{v} = \frac{1}{2(1+h)\,G_0}\frac{d\tilde{p}}{d\xi} + g_1(z)\,\xi + g_2(z), \tag{4.9}$$

$$\tilde{w} = -\frac{z}{4(1+h)\,G_0}\frac{d^4\tilde{p}}{d\xi^4} + \delta(\xi), \tag{4.10}$$

$$\tilde{T} = -\frac{h}{(1+h)\,G_0}\frac{d\tilde{p}}{d\xi} + 2\{g_1(z)\,\xi + g_2(z)\}, \tag{4.11}$$

where $g_1(z)$, $g_2(z)$ and $\delta(\xi)$ are unknown functions. To determine $\tilde{P}$ and δ we must investigate the Ekman layers of the $E^{\frac{1}{4}}$-layer, called Ekman extensions, on the top and bottom end plates. The Ekman extensions have the same structure as the Ekman layer treated in § 3 and we do not write down the equations. The solutions in the Ekman extensions are

$$\tilde{u} = -\tfrac{1}{2}(1+h)^{\frac{1}{2}} D_{\pm}(\xi)\, e^{-\hat{\sigma}\eta} \sin \hat{\sigma}\eta, \tag{4.12}$$

$$\tilde{v} = -\tfrac{1}{2} D_{\pm}(\xi)\, e^{-\hat{\sigma}\eta} \cos \hat{\sigma}\eta, \tag{4.13}$$

$$\tilde{w} = \tfrac{1}{4} j(1+h)^{\frac{1}{2}} (dD_{\pm}(\xi)/d\xi)\, e^{-\hat{\sigma}\eta}(\cos \hat{\sigma}\eta + \sin \hat{\sigma}\eta), \tag{4.14}$$

$$\tilde{T} = D_{\pm}(\xi)\, e^{-\hat{\sigma}\eta} \cos \hat{\sigma}\eta \quad \text{on} \quad z = \pm A, \tag{4.15}$$

where $\hat{\sigma} = (1+h)^{\frac{1}{4}}$. The boundary conditions are

$$\frac{\partial \tilde{T}}{\partial z} - j\beta \frac{\partial \hat{T}}{\partial \eta} = 0, \quad \tilde{v} + \hat{v} = j\omega, \quad \tilde{w} + \hat{w} = 0 \quad \text{at} \quad z = \pm A, \tag{4.16}$$

where we regard the quantities with tildes as ones including the components of solutions in the inner inviscid core. Substituting (4.9)–(4.11) and (4.13)–(4.15) into (4.16), we have

$$2\{g_1'(\pm A)\,\xi + g_2'(\pm A)\} \pm \beta\sigma D_{\pm}(\xi) = 0, \tag{4.17}$$

$$\frac{1}{2(1+h)\,G_0} \frac{d\tilde{p}}{d\xi} + g_1(\pm A)\,\xi + g_2(\pm A) - \tfrac{1}{2} D_{\pm}(\xi) = \pm \omega, \tag{4.18}$$

$$\mp \frac{A}{4(1+h)\,G_0} \frac{d^4\tilde{p}}{d\xi^4} + \delta(\xi) \pm \tfrac{1}{4}(1+h)^{\frac{1}{2}} \frac{dD_{\pm}(\xi)}{d\xi} = 0. \tag{4.19}$$

From (4.17) and (4.18) we can see immediately that $d\tilde{p}/d\xi$ is a linear function of ξ and, therefore, we can not have solutions of boundary-layer type. It should be noted that the fact of there being no $E^{\frac{1}{4}}$-layer is particular to the present case of thermally insulated end plates and imposes one condition on the solution in the inner inviscid core.

The analysis of the $E^{\frac{1}{3}}$-layer is the same as in I and we do not go into the details here. The essential features of the $E^{\frac{1}{3}}$-layer components of solutions are as follows: (i) since the temperature distribution on the side wall is antisymmetric with respect to z, the solutions $\bar{v}$ and $\overline{T}$ are expressed as antisymmetric functions of z expanded in Fourier series, where bars refer to the $E^{\frac{1}{3}}$-layer, (ii) the relation

$$2h\bar{v} + \overline{T} = 0 \tag{4.20}$$

holds.

On the other hand, the boundary conditions on the side wall are expressed by

$$v_i + \bar{v} = 0, \quad T_i + \overline{T} = z/A. \tag{4.21), (4.22}$$

Combining (2.12) and (4.20)–(4.22) and noting that $\bar{v}$ and $\overline{T}$ are antisymmetric functions of z, we conclude that

$$f(1) = 0 \tag{4.23}$$

and

$$T_i = z/A(1+h) \quad \text{at} \quad r = 1. \tag{4.24}$$

The condition $f(1) = 0$ is due to the fact that there is no $E^{\frac{1}{4}}$-layer in the present problem through which the symmetric part of the solutions could be linked with the boundary conditions on the side wall (see Hunter 1967).

Before proceeding further, it may be useful to consider for what cases condition (4.23) is satisfied. Substituting (4.24) into (3.23), we obtain

$$f(1) = -C_s(1) = -2\sigma(1)^{-1}\int_0^1 r\epsilon_R(w_+ - w_-)\,dr. \tag{4.25}$$

The condition (4.23) implies, then, that the total mass flux of fluid into the centrifuge through the horizontal end plates must be zero. This is satisfied in most cases except a case in which the fluid is injected or extracted through the boundary within the side-wall boundary layer. In this paper we do not treat this exceptional case, although it is interesting to study how to match the symmetric part $f(1)$, of the solutions in the inner inviscid core with the boundary condition on the side wall without the $E^{\frac{1}{4}}$-layer.

5. The inner temperature field

Our problem reduces now to obtaining the inner temperature distribution T_i from the governing equation (2.13) and boundary conditions (3.17) and (4.24), which couples with (3.22), (3.23) and the condition (4.23). In order to solve (2.13), we decompose T_i as follows:

$$T_i(r,z) = T_0(r) + zA^{-1}(1+h)^{-1} + \Phi(r,z), \tag{5.1}$$

where $T_0(r)$ is a particular solution of (2.13) and $\Phi(r,z)$ a solution of its homogeneous counterpart. As in II, a formal solution for $T_0(r)$, under the conditions $T_0(1) = T_0'(0) = 0$, is

$$T_0(r) = -h\int_r^1 t^{-1}(1+ht^2)^{-1}dt\int_0^t s^2\mathscr{L}f\,ds. \tag{5.2}$$

The homogeneous solution Φ should not be singular at $r = 0$ and must satisfy the boundary condition $\Phi(1,z) = 0$. Let us expand Φ in terms of a symmetric part and an antisymmetric part according to

$$\Phi(r,z) = \sum_{n=1}^{\infty}\left\{a_n\frac{\cosh(\lambda_n z)}{\cosh(\lambda_n A)} + b_n\frac{\sinh(\lambda_n z)}{\sinh(\lambda_n A)}\right\}g_n(r), \tag{5.3}$$

leading to the Sturm–Liouville problem for (g_n, λ_n), i.e.

$$\left.\begin{aligned} &\frac{d}{dr}\left\{r(1+hr^2)\frac{dg_n}{dr}\right\} + \lambda_n^2 r g_n = 0, \\ \text{with}\quad &g_n = 0 \quad \text{at} \quad r = 1, \quad dg_n/dr = 0 \quad \text{at} \quad r = 0. \end{aligned}\right\} \tag{5.4}$$

By the Sturm–Liouville theorem, (5.4) possesses a complete set of solutions which can be used to represent any function of r. If we neglect h, (5.4) reduces to the Bessel equation of zero order. The normalized eigenfunctions g_n and the eigenvalues λ_n reduce to $2^{\frac{1}{2}}J_0(j_{0n}r)/J_1(j_{0n})$ and j_{0n}, respectively, where J_m is an mth-order Bessel function and j_{0n} is the nth zero of J_0. These functions will be used to obtain numerical results in the next section.

The unknown constants a_n and b_n are determined from the boundary condition (3.17). Inserting (5.1) and (5.3) into (3.17), we obtain two equations, and addition of these two equations yields

$$\sum_{n=1}^{\infty} a_n \lambda_n \tanh(\lambda_n A) g_n(r) = -\beta\sigma(r) C_s(r), \tag{5.5}$$

where use has been made of (3.23). Subtraction of the two equations gives

$$\sum_{n=1}^{\infty} b_n \{\beta\sigma r^2 + \lambda_n \coth(\lambda_n A)\} g_n(r) = -\frac{\beta\sigma r^2 + A^{-1}}{1+h} + 2\beta\sigma r^2\omega. \tag{5.6}$$

Using the orthogonality of the set $g_n(r)$, we multiply (5.5) and (5.6) by $rg_m(r)$ and integrate them from 0 to 1 to obtain

$$a_n = -2\beta\lambda_n^{-1} \coth(\lambda_n A) \int_0^1 rg_n(r)\,dr \int_0^r r\epsilon_R(w_+ - w_-)\,dr \tag{5.7}$$

and

$$\beta \sum_{m=1}^{\infty} b_m \int_0^1 \sigma(r) r^3 g_n(r) g_m(r)\,dr + b_n \lambda_n \coth(\lambda_n A)$$
$$= -\beta(1+h)^{-1} \int_0^1 \sigma(r) r^3 g_n(r)\,dr - A^{-1}(1+h)^{-1} \int_0^1 rg_n(r)\,dr$$
$$+ 2\beta\omega \int_0^1 \sigma(r) r^3 g_n(r)\,dr. \tag{5.8}$$

Equations (5.8) form an infinite set of linear algebraic equations. The first and second terms on the right-hand side of (5.8) are due to the applied temperature gradient on the side wall, while the third term is due to the differential rotation of the end plates. The terms including β are due to the compressibility of the fluid and the thermal insulation of the end plates.

6. Numerical examples

Thermally driven flow

Here we give numerical examples of the flow induced when we include only the linear temperature distribution on the side wall, i.e. no source–sink distribution or differential rotation of the end plates is assumed. Since the inner temperature field is, in this case, an antisymmetric function of z, we find that a_n, $f(r)$, $C_s(r)$ and $T_0(r)$ are identically zero. The function $C_a(r)$ is written simply as

$$C_a(r) = r^2 \left\{ \sum_{n=1}^{\infty} b_n g_n(r) + (1+h)^{-1} \right\}. \tag{6.1}$$

Substitution of (6.1) into (3.20) yields

$$w_i = -\frac{1}{8} \frac{(1+hr^2)^{\frac{1}{2}}}{\sigma} \left\{ \left(4 + G_0 r^2 + \frac{hr^2}{1+hr^2}\right) \left(\sum_{n=1}^{\infty} b_n g_n(r) + \frac{1}{1+h} \right) + 2r \sum_{n=1}^{\infty} b_n g_n'(r) \right\}, \tag{6.2}$$

where the prime denotes differentiation with respect to r.

As in III we solve the equations neglecting h but retaining β ($= hE^{-\frac{1}{2}}$). In this approximation, g_n reduces to the well-known Bessel function as pointed

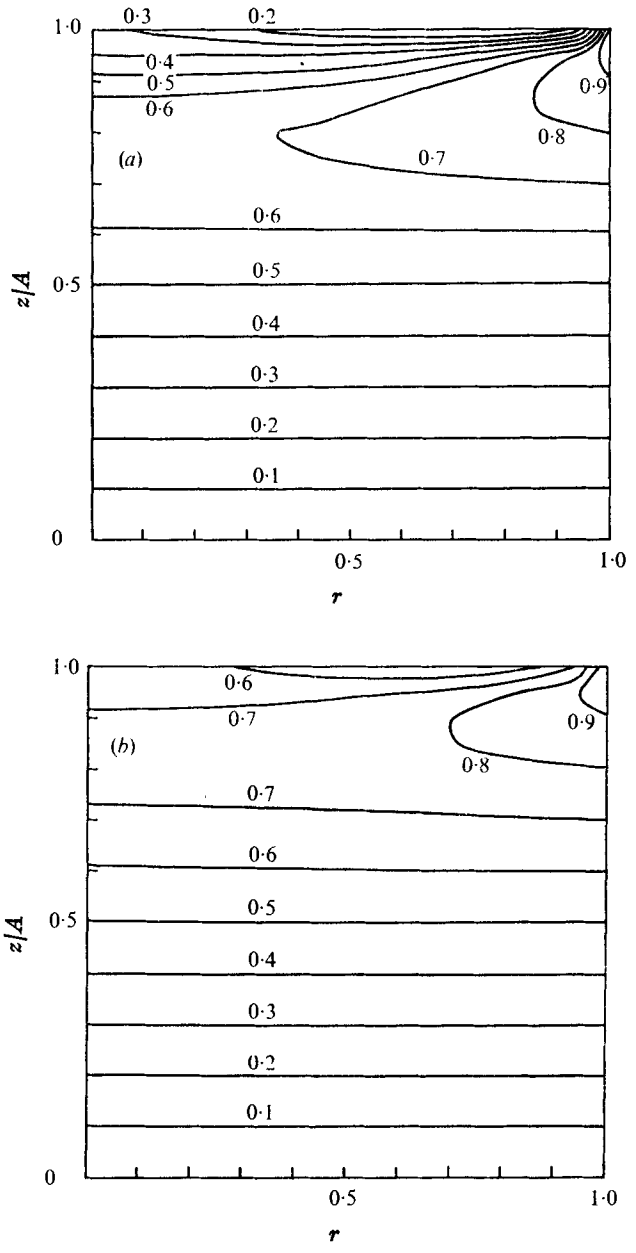

FIGURES 1(*a*, *b*). For legend see facing page.

out in the preceding section. The problem is now to solve an infinite set of linear algebraic equations for b_n, viz. (5.8), under the condition $\omega = 0$. These equations are solved numerically by truncating after the first 80 terms. The coefficient b_n is then found to have converged sufficiently.

Figure 1 shows the temperature distribution for the cases $G_0 = 0$, 0·01, 0·1 and 1. The values of β corresponding to these values of G_0 are 0, 0·053, 0·53 and 5·3,

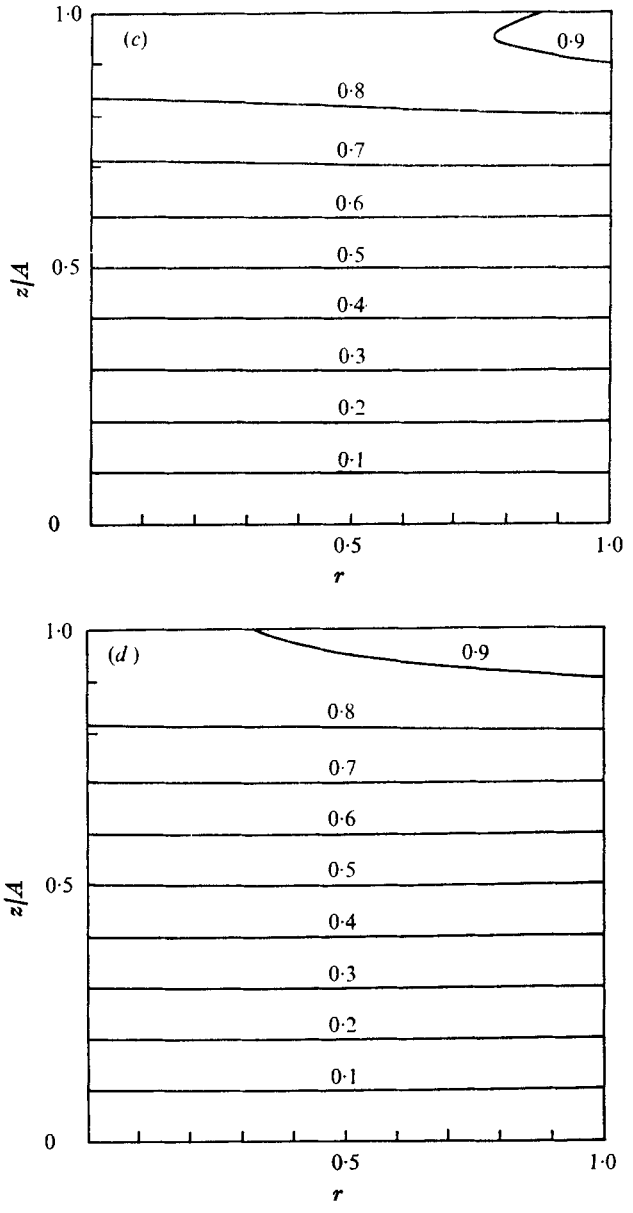

FIGURE 1. The temperature fields in the inner inviscid cores of thermally driven flows. (*a*) $G_0 = 1$, (*b*) $G_0 = 0{\cdot}1$, (*c*) $G_0 = 0{\cdot}01$, (*d*) $G_0 = 0$.

respectively. In all numerical calculations the values of γ, P_r, E and A are set to be 1·067, 1, 10^{-7} and 5. The axial velocity profiles w_i are shown in figure 2.

Mechanically driven flow

We next consider numerical examples of mechanically driven flow caused only by an antisymmetric differential rotation of the end plates, i.e. $v = \pm r\omega$ on $z = \pm A$. No source–sink distribution is assumed and $T = 0$ on the side wall.

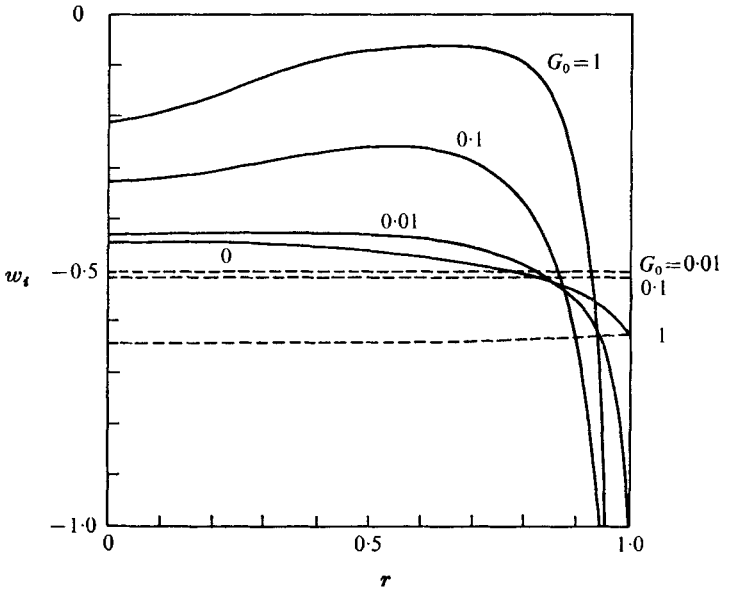

FIGURE 2. The axial velocity profiles for thermally driven flows. – – –, axial velocity profiles for the case in which the end plates are not thermally insulated but have a constant temperature distribution, i.e. $T = \pm 1$ at $z = \pm A$.

Then the inner temperature field is antisymmetric with respect to z and we find $f(r)$, $C_s(r)$ and $T_0(r)$ are identically zero. Also we drop the second term in (5.1) since the side-wall temperature gradient is not applied. The functions $C_a(r)$ and w_i reduce to

$$C_a(r) = r^2\left\{\sum_{n=1}^{\infty} b_n g_n(r) - 2\omega\right\}, \tag{6.3}$$

$$w_i = -\frac{1}{8}\frac{(1+hr^2)^{\frac{1}{2}}}{\sigma}\left\{\left(4+G_0 r^2+\frac{hr^2}{1+hr^2}\right)\left(\sum_{n=1}^{\infty} b_n g_n(r)-2\omega\right)+2r\sum_{n=1}^{\infty} b_n g_n'(r)\right\}. \tag{6.4}$$

If we put $\omega = -\frac{1}{2}$ and neglect h, (6.3) and (6.4) reduce to (6.1) and (6.2), respectively. In the limit $G_0 \to 0$, which is the incompressible limit, b_n is identically zero and w_i has the constant value ω. In figures 3 and 4, the inner temperature field and the axial velocity profiles are shown for purely mechanically driven flows based on numerical calculations which used truncation after 80 terms and $\omega = -\frac{1}{2}$.

Externally driven flow

Here we consider the flow driven only by a source–sink distribution on the end plates. There is no differential rotation of the end plates, i.e. $\omega = 0$, and $T = 0$ on the side wall. The inner temperature is symmetric with respect to z, and we can neglect b_n and $C_a(r)$; and again we drop the second term in (5.1). As $C_s(r)$ and a_n are solved explicitly in (3.22) and (5.7), it is straightforward to compute Φ and obtain T_i. Substituting this into (3.23), we obtain

$$f(r) = r\left\{\sum_{n=1}^{\infty} a_n g_n(r) + T_0(r)\right\} - r^{-1}C_s(r). \tag{6.5}$$

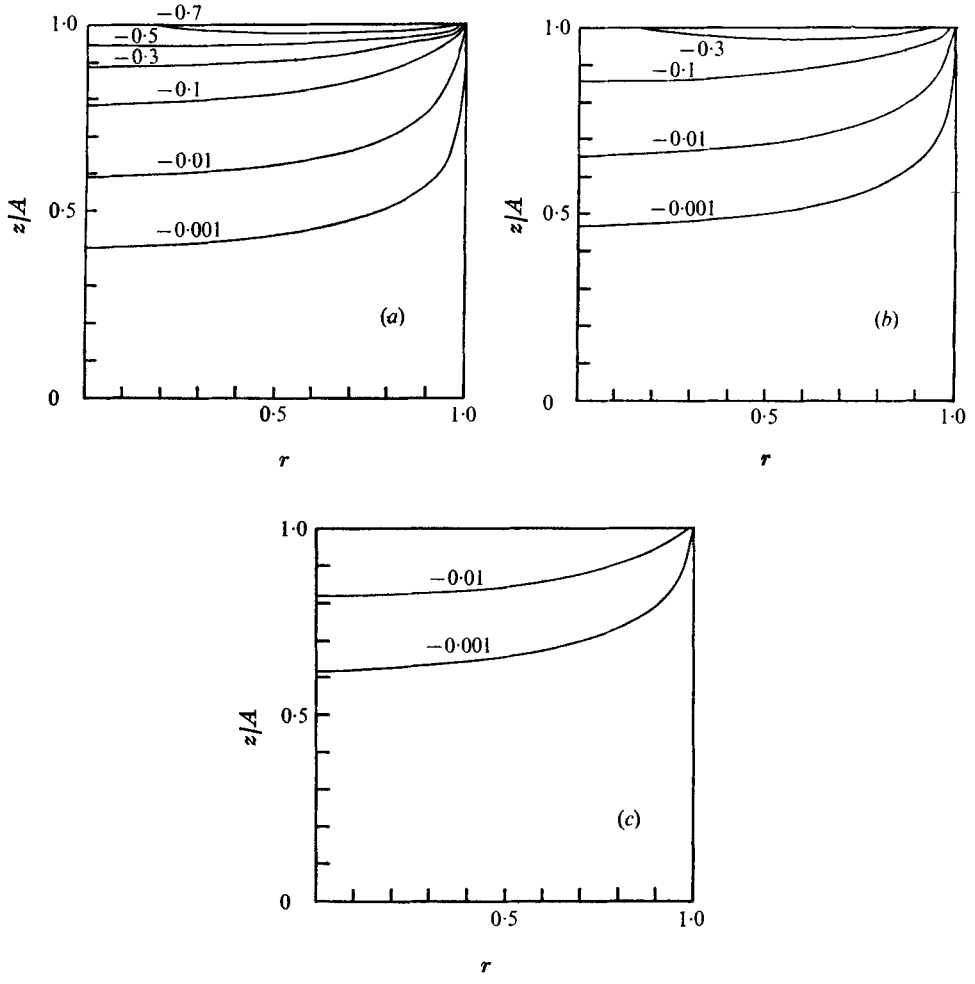

FIGURE 3. The temperature fields in the inner inviscid cores of mechanically driven flows. (*a*) $G_0 = 1$, (*b*) $G_0 = 0{\cdot}1$, (*c*) $G_0 = 0{\cdot}01$.

Combining (6.5) with (5.2), we get an integro-differential equation for $f(r)$ or $T_0(r)$. In the present approximation of small h, however, $T_0(r)$ can be neglected compared with $f(r)$ because the order of magnitude of $T_0(r)$ is $hf(r)$ [see (5.2)].

As for the source–sink flow profile on the end plates $w_\pm(r)$, let us assume that these functions are expressed by delta functions. This means that the width of the source–sink slits is very narrow. In reality, this simplification violates our basic assumption that $w_\pm(r)$ are smooth functions of r and in that case we must consider Stewartson's $E^{\frac{1}{3}}$- and $E^{\frac{1}{4}}$-layers which occur on the slits (Nakayama & Usui 1974; Hashimoto 1975). However, as far as the overall structure of the solution is concerned, there is no significant difference.

As an example of a source–sink distribution we take a configuration schematically shown in figure 5. An inner slit is located at $r = r_1$. Outer slits are located at $r = 1$ but just outside the $E^{\frac{1}{3}}$-layer on the side wall to satisfy the condition (4.23).

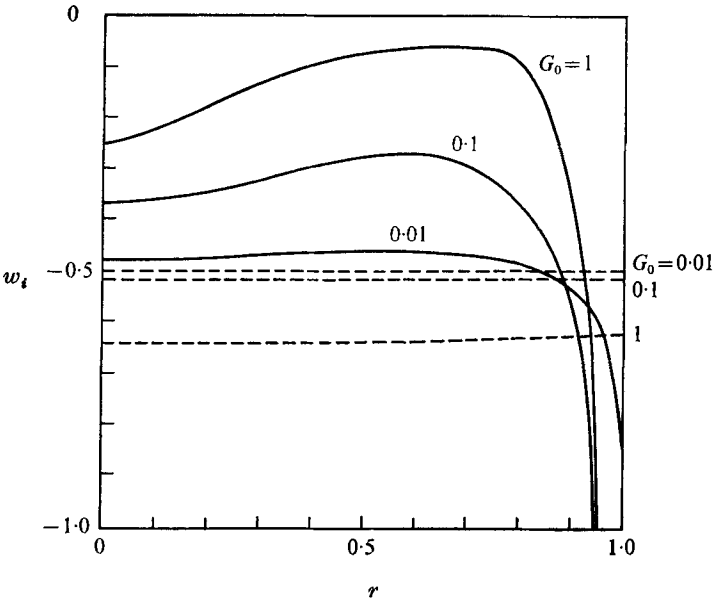

FIGURE 4. The axial velocity profiles for mechanically driven flows with $\omega = -\frac{1}{2}$. ---, axial velocity profiles for the case in which the end plates have a constant temperature distribution, i.e. $T = 0$ at $z = \pm A$.

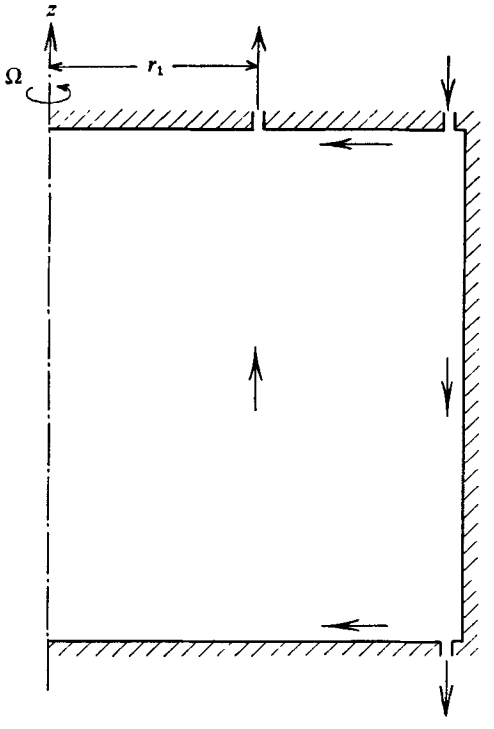

FIGURE 5. The inflow and outflow configuration.

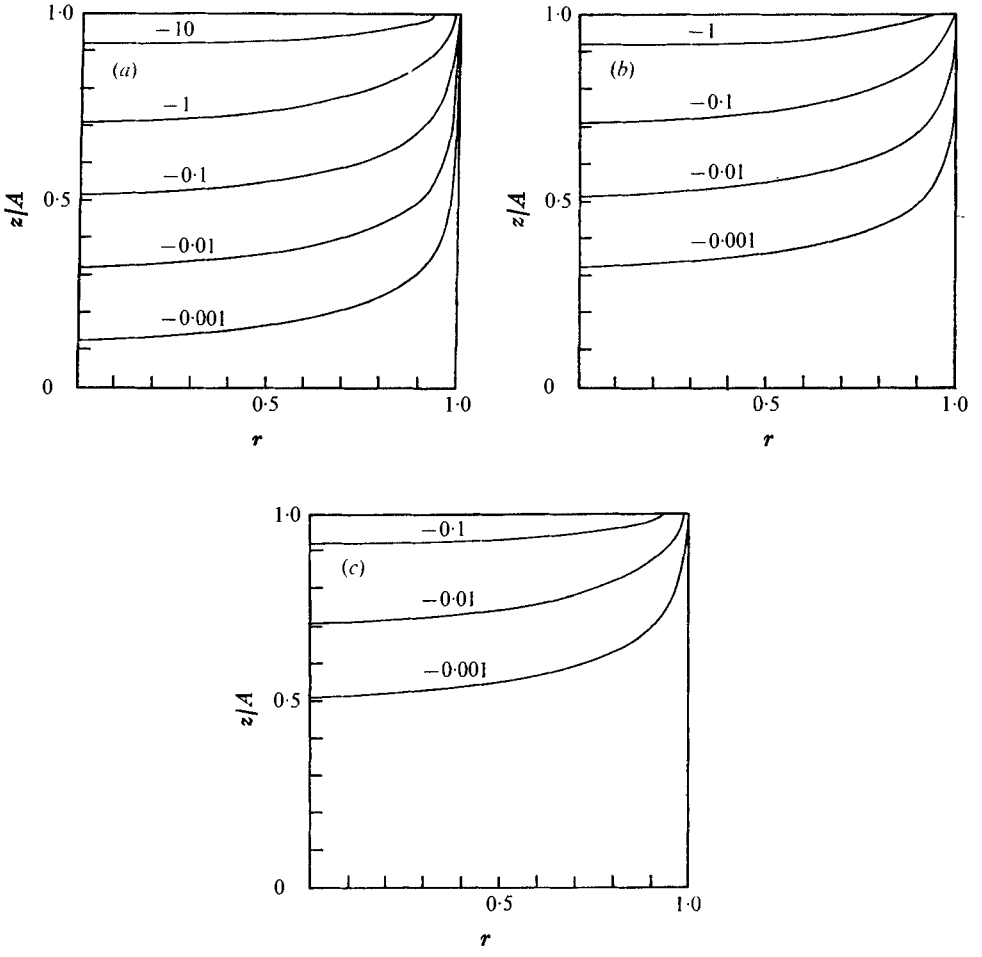

FIGURE 6. The temperature fields in the inner inviscid cores of externally driven flows. (*a*) $G_0 = 1$, (*b*) $G_0 = 0{\cdot}1$, (*c*) $G_0 = 0{\cdot}01$.

In this case, we have

$$\int_0^r re_R(w_+ - w_-)\,dr = \begin{cases} 0 & \text{for} \quad 0 \leqslant r < r_1, \\ \Lambda & \text{for} \quad r_1 < r < 1, \\ 0 & \text{at} \quad r = 1, \end{cases} \tag{6.6}$$

where Λ is a constant related to the amount of influx. Substitution of (6.6) into (5.7) yields

$$a_n = -2a\beta\lambda_n^{-1} \coth(\lambda_n A) \int_{r_1}^1 r g_n(r)\,dr. \tag{6.7}$$

In the numerical calculations, we take $r_1 = 0{\cdot}5$ and $\Lambda = 1$.

The inner temperature fields are shown in figure 6. The inner axial profile of w_i is obtained from (3.20) as

$$w_i = \tfrac{1}{2}(w_+ + w_-), \tag{6.8}$$

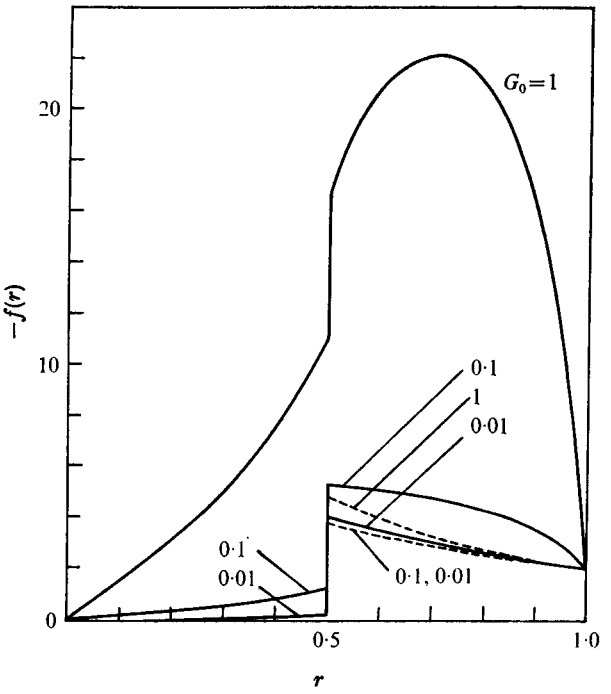

FIGURE 7. The profiles of $f(r)$ $(= -G_0^{-1}dp_i/dr)$. The jumps at $r = \frac{1}{2}$ and 1 are due to the influx given by the delta function. ---, the profiles when the end plates have a constant temperature distribution $T = 0$ at $z = \pm A$, in which case $f(r) = -2r^{-1}\sigma^{-1}\int_0^r r\epsilon_R(w_+ - w_-)\,dr$.

which is determined only by the source–sink distribution and is not affected by the thermal conditions on the end plates. Therefore, instead of showing the axial flow profile, we give the distribution of the inner pressure gradient in figure 7.

7. Concluding remarks

The radial fluid motion in the Ekman layers causes volume changes in the fluid elements which in turn produce heat. This heat is absorbed through the end plates when they are thermally conducting; while, if the end plates are insulated, heat absorption through the end plates is prohibited and therefore the radial motions are suppressed. This, in turn, leads to the suppression of the axial flow in the inner inviscid core.

To examine the effects of the thermal insulation of the end plates, we compare the results obtained in the last section with those of the conducting end plates. In figures 2, 4 and 7 the continuous lines refer to the insulated end plates and the dashed lines refer to the conducting end plates, on which the temperature is fixed at a certain constant value. Figures 2 and 4 show the profiles of w_i for the thermally driven case and the mechanically driven case, respectively. We can see the suppression of the axial flow in the greater part of the inner core except the region near the side wall. The large axial flow near the side wall indicates

the existence of large radial motions in the corresponding regions of the Ekman layers. These large radial motions must be maintained by the heat supply from the side wall because the end plates are thermally insulated. The large heat flux from the side wall to the Ekman layer in the corner regions at $r = 1$ and $z = \pm A$ can be seen in figures 1 and 3. Figure 7 shows the distribution of $f(r)$, which is equal to $-G_0^{-1}dP_i/dr$ for the externally driven case. The differences between the continuous lines and the dashed lines become larger as G_0 increases. This implies that, as G_0 increases, the pressure difference between the inner slit and outer slits required to maintain the same amount of source–sink flow is greater for thermally insulated end plates than for conducting end plates, because of the predominance of the suppression of the radial fluid motion in the Ekman layer.

The conclusion that the thermal conditions on the end plates have a direct influence on the axial flow is quite different from that obtained in III, in which it was found that the thermal condition on the side wall affects the inner temperature fields but not the axial flow when the end plates are thermally conducting. For the separation of uranium isotopes by the gas centrifuge, the distribution of the isotopes is calculated from the axial flow profile. Hence, from the practical point of view, the evaluation of the thermal condition of the end plates is an important problem.

A distinctive feature of the present problem is that there is no $E^{\frac{1}{4}}$-layer, whether T_i and v_i at $r = 1$ or the T and v given as side-wall boundary conditions have symmetric parts or not (in the strict sense of the term, 'symmetric part' means the constant part when the solutions are expanded in Fourier series with respect to z). So far, the role of the $E^{\frac{1}{4}}$-layer has been understood as connecting the constant parts of the inner solutions and the side-wall boundary conditions. We can not expect this matching by the $E^{\frac{1}{4}}$-layer in the present problem and this leads to one condition: the corresponding constant parts must be equal to each other. In this paper we restricted ourselves to the case in which this condition is satisfied. However, as is mentioned at the end of § 4, the condition is not always satisfied and the present authors have been investigating the problem of how to match the solutions at the side wall in such a exceptional case.

The authors would like to thank Prof. T. Sakurai for valuable discussions. One of the authors (T.M.) is grateful to Prof. N. C. Wickramasinghe for providing a chance to visit the U.K. under an S.R.C. Visiting Fellowship. He is also grateful to Dr A. H. Nelson for a careful reading of the manuscript. The numerical calculations were made on the FACOM 230-60 electric computer of the Data Processing Center of Kyoto University.

REFERENCES

Cohen, K. P. 1951 *The Theory of Isotope Separation as Applied to the Large Scale Production of* U-235. McGraw-Hill.

Hashimoto, K. 1975 A source–sink flow in an incompressible rotating fluid. *J. Phys. Soc. Japan*, **38**, 1508–1515.

Homsy, G. M. & Hudson, J. L. 1969 Centrifugally driven thermal convection in a rotating cylinder. *J. Fluid Mech.* **35**, 33–52.

HUNTER, C. 1967 The axisymmetric flow in a rotating annulus due to a horizontally applied temperature gradient. *J. Fluid Mech.* **27**, 753–778.

KANAGAWA, K. & OYAMA, Y. 1961 On the isotope separation by counter-current gas centrifuge. *J. Atom. Energy Soc. Japan*, **3**, 868–922. (See also *ibid.* **3**, 918–922; in Japanese.)

MATSUDA, T., SAKURAI, T. & TAKEDA, H. 1975 Source–sink flow in a gas centrifuge. *J. Fluid Mech.* **67**, 197–208.

MATSUDA, T. 1975 Isotope separation by thermally driven countercurrent gas centrifuge. *J. Nucl. Sci. Tech.* **12**, 512–518.

MATSUDA, T., HASHIMOTO, K. & TAKEDA, H. 1976 Thermally driven flow in a gas centrifuge with an insulated side wall. *J. Fluid Mech.* **73**, 389–399.

NAKAYAMA, W. & USUI, S. 1974 Flow in rotating cylinder of gas centrifuge. *J. Nucl. Sci. Tech.* **11**, 242–262.

OLANDER, D. R. 1972 Technical basis of the gas centrifuge. *Adv. Nucl. Sci. Tech.* **6**, 105–174.

SAKURAI, T. & MATSUDA, T. 1974 Gasdynamics of a centrifugal machine. *J. Fluid Mech.* **62**, 727–736.

STEWARTSON, K. 1957 On almost rigid rotations. *J. Fluid Mech.* **3**, 17–26.